

# Coupler-induced errors for flux-qubit quantum annealer: measurements for one-dimensional Ising model with twisted boundary fields

Nicholas Chancellor<sup>\*%</sup>, Philip J. D. Crowley<sup>\* $\mathcal{L}$</sup> , Tanja Đurić<sup>\* $\mathcal{S}$</sup> , Walter Vinci<sup>\* $\sim$</sup>   
 Mohammad H. Amin<sup>” $\dagger$</sup> , Andrew G. Green<sup>\*</sup>, Paul A. Warburton<sup>\* $\wedge$</sup> , and Gabriel Aeppli<sup>&</sup>

June 3, 2022

<sup>\*</sup>London Centre For Nanotechnology, University College London 19 Gordon Street, London UK, WC1H 0AH

<sup>“</sup> D-Wave Systems Inc. 3033 Beta Avenue Burnaby, British Columbia, Canada V5G 4M9

<sup>&</sup>Physics Department, ETH Zürich, Switzerland CH-8093; Institut de Physique, EPFL, Lausanne, Switzerland CH-1015; Paul Scherrer Institute, Villigen, Switzerland CH-5232

<sup>$\dagger$</sup> Department of Physics, Simon Fraser University, Burnaby, BC Canada V5A 1S6

<sup>$\wedge$</sup> Department of Electronic and Electrical Engineering, UCL, Torrington Place London UK WC1E 7JE

<sup>%</sup> current affiliation: Department of Physics, Durham Newcastle Joint Quantum Centre, Durham University, South Road, Durham, DH1 3LE

<sup>$\mathcal{L}$</sup>  current affiliation: Department of Physics, Boston University, Boston, MA 02215, USA

<sup>$\mathcal{S}$</sup>  current affiliation: Department of Physics, Faculty of Science, University of Zagreb, Bijenička c. 32, 10000 Zagreb, Croatia

<sup>$\sim$</sup>  current affiliation: Quantum Artificial Intelligence Lab. (QuAIL), NASA Ames Research Center, Moffett Field, CA 94035, USA KBR, 601 Jefferson St., Houston, TX 77002, USA

## Abstract

A finite length ferromagnetic chain with opposite spin polarisation imposed at its two ends is one of the simplest frustrated spin models. In the clean classical limit the domain wall inserted on account of the boundary conditions resides with equal probability on any one of the bonds, and the degeneracy is precisely equal to the number of bonds. If quantum mechanics is introduced via a transverse field, the domain wall will behave as a particle in a box, and prefer to be nearer the middle of the chain rather than the ends. A simple characteristic of a real quantum annealer is therefore which of these limits obtains in practice. Here we have used the ferromagnetic chain with antiparallel boundary spins to test a real flux qubit quantum annealer and discover that contrary to both expectations, the domain walls found are non-uniformly distributed on account of effective random longitudinal fields present notwithstanding tuning carried out to zero out such fields when the couplings between qubits are nominally zero. We present a simple derivation of the form of the distribution function for the domain walls, and show also how the effect we have discovered can be used to determine the strength of the effective random fields (noise) characterising the annealer. The noise measured in this fashion is smaller than what is seen during the single qubit tuning process, but nonetheless qualitatively affects the outcome of the simulation performed by the annealer.

## Introduction

The low energy states of natural systems can correspond to the solutions of computationally difficult problems [1]. Experiments suggest that these low energy states can be accessed and measured by taking advantage of quantum mechanics, using a technique known as quantum annealing [2]. Here, the "difficult" problem is converted to an equivalent problem of finding the ground state of an Ising Hamiltonian, and that classical ground state is approached via the introduction and subsequent removal of quantum fluctuations, typically imposed via transverse fields. It is suspected but by no means universally agreed that quantum annealing could provide an improvement over other methods for certain classes of interesting problems [3, 4]. To harness the power of quantum annealing, machines must be constructed to faithfully implement the relevant transverse field Ising Hamiltonian (TFIM), and to do so represents a major challenge in quantum information science and engineering. We refer to such machines as annealers. While the eventual outputs of annealers usually take discrete binary values, the control parameters, which are the coupling constants in the TFIM, must be chosen from a continuous set of values. An annealer should therefore be considered an analog rather than a digital computer.

Quantum annealing has attracted considerable experimental attention recently [6, 7, 8, 9, 10, 11, 12, 13], which is understandable given the wide variety of applications, from traditional computer science problems [12, 14], to more exotic uses such as aiding genetic algorithms to calculate radar waveforms [13], search engine ranking [15], graph isomorphism [10], and portfolio optimization [16]. In addition, sampling using a quantum annealer, which is effectively the topic of the current paper, is highly relevant to many machine learning and statistical inference tasks [17, 18, 19, 20, 21, 22, 23].

Precision of control parameters is a fundamental issue in analog computing, not present in its digital counterpart [24]. It is therefore important to ask what new complications these errors may add. One could hope, for example, that small uncorrelated control errors simply average out, leading to no no-

ticeable effect as long as they are below a threshold [25]. Long timescale noise should also be considered a source of control error; this noise will be indistinguishable from the TFIM being mis-specified by the device. We demonstrate here that the effects of control errors can be counter-intuitive, giving non-uniform distributions within a degenerate manifold even for uncorrelated errors. We further argue that this effect captures error-causing noise that would be missed if we try to measure the errors with a different protocol.

There is a growing literature on error correction in quantum annealing. Most of the studies focus upon the effect of coupling to an external bath rather than control errors [26, 28, 29, 30, 31]. The work in [25, 39, 32] does mention techniques that can reduce the effect of control errors, at the cost of some overhead, but cannot completely eliminate them. For the purposes of this study there are two kinds of relevant noise processes, the dissipation which occurs on a time scale comparable or faster than the system dynamics, and slower noise which appears fixed with respect to these timescales and acts as effective random field terms. The role of the faster noise is to hasten relaxation to a thermal distribution, while the slower noise (referred to as control errors) is what is directly measured in the experiments we report.

While the present study is dedicated to the consequences rather than the physical origins of the noise in flux qubit quantum annealers, we note other literature describing this noise as due to interactions of the qubit with magnetic defects in the chip substrate [34]. It typically takes a profile with a  $\frac{1}{f}$  type frequency profile, meaning that the noise contains both high and low frequency components. The low frequency components can be treated as effectively static control errors, and are responsible for the effects that we report here.

We examine experimentally the effect of control errors on the annealer constructed by D-Wave Systems, which mimics an Ising spin system. Our experiment shows a non-uniform distribution within a ground state manifold that can be explained by classical Boltzmann distributions under the influence of field control errors, demonstrating that even small errors affect the solution to strikingly simple problems.

The fact that such a simple system subject to uniform noise can produce a non-uniform, but regular and predictable distribution, is an interesting mathematical result on its own, and to the best of our knowledge has not been previously reported in the literature.

We find that even a domain wall in a one-dimensional system subject to *uncorrelated* field control errors yields a non-trivial U-shaped domain wall distribution. An effective potential for the domain walls is generated by combinatoric effects in the averaging over disorder in the Hamiltonian. In this sense the phenomenon that we observe is due to an entropic potential. While the average domain-wall energy is the same at every site; there are more field configurations where the lowest energy spin configuration has the domain wall near the ends, the probability of observing it in such positions is higher. This is a finite size effect distinguishable from order-by-disorder which occurs in infinite systems, where the term was originally used [5] to describe entropic effects in the thermodynamic limit. We further demonstrate that this distribution can be used to measure noise in the device and discuss the advantages over the conventional method of examining single qubit auto-correlation.

The hardware that we use implements a transverse field Ising model with a time-dependent Hamiltonian of the form,

$$H(t) = -A(t) \sum_{i=1} \sigma_i^x + B(t) H_{\text{prob}}, \quad (1)$$

where  $H_{\text{prob}}$  is a user-specified Ising Hamiltonian, which is diagonal in the  $z$  basis, and  $A(t)$ ,  $B(t)$  are the annealing schedule, the time dependences that control the relative strength of each term.

The specific problem that we choose to study is a ferromagnetic chain with opposing fields at either end as shown in Fig. 1. As long as  $|h| > J > 0$ ,  $H_{\text{prob}}$  will have an  $(N - 1)$ -fold degenerate ground state manifold consisting of all states with a single domain wall;  $|\uparrow\downarrow\downarrow\ldots\downarrow\rangle, |\uparrow\uparrow\downarrow\ldots\downarrow\rangle \ldots |\uparrow\uparrow\ldots\uparrow\downarrow\rangle$ . This same system has been shown in [42, 43] to be an effective method to encode discrete variables, and has been shown experimentally to improve performance

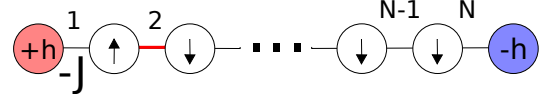


Figure 1: Illustration of the Hamiltonian showing one of the ground states assuming that  $h > J$  and the qubits on the end satisfy the applied fields. Numbers indicate domain-wall sites.

in optimisation [44, 45]. In our experiments, we use  $h = 2J$  with a Hamiltonian of the form

$$H_{\text{prob}} = J \sum_{i=1}^N -\sigma_i^z \sigma_{i+1}^z + h (\sigma_1^z - \sigma_{N+1}^z). \quad (2)$$

We focus on control errors arising from stray magnetic fields from free spins and dangling bonds within the materials that make up the quantum processing unit (QPU). This could be considered equivalent to adding a term of the form,

$$H_{\text{fields}} = \sum_i \zeta_i \sigma_i^z, \quad (3)$$

to the overall Hamiltonian, where  $\zeta_i$  are uncorrelated and Gaussianly distributed with a standard deviation  $\sigma_\zeta \ll J$  and zero mean  $\overline{\zeta_i} = 0$ . The overline indicates an ensemble average. Random field terms such as those in Eq. 3 appear naturally in implementations of the transverse field Ising model, including for example the dipole-coupled magnet  $\text{LiHo}_x\text{Y}_{1-x}\text{F}_4$  [35]. Because the coupling between the qubits and the substrate is likely to change with bias,  $\zeta_i$  will generally be time-dependent, however as we show later the system remains in thermal equilibrium until very late in the anneal, so it may be treated as static for the purpose of these experiments.

One can also consider coupler control errors of the form  $H = \sum_i \zeta_i^{(J)} \sigma_i^z \sigma_{i+1}^z$ , where  $\zeta_i^{(J)}$  satisfy the same conditions as  $\zeta_i$  with a standard deviation  $\sigma_J \ll J$ . This type of control error produces an uncorrelated potential for the domain walls, and therefore has no effect upon the shape of the mean thermal domain-wall distribution. We demonstrate this in Sec. 2.1 of the supplemental material. It is worth noting briefly that [8] describes a similar experiment, but with the goal of demonstrating quantum

tunneling, as had been done previously for a disordered magnet [36]. A qualitatively similar domain wall distribution to the one that we see can be found in the supplemental material of [8], although there is no discussion of this finding and its possible origins.

One concept that helps explain the behaviour of these systems is *freeze time*, which is the time at which the dynamics of the QPU effectively stop and the spins are effectively fixed. Because the device appears to be reaching thermal equilibrium in these experiments, we can think of these experiments as measuring the ratio of the noise level to the device temperature at the freeze time. Since the susceptibility of flux qubits to external noise will, in general, be different at different points in the experiment, the freeze time is an important (but not directly measurable) parameter.

Beyond control parameter errors, there is the quantum mechanical effect of zero point fluctuations which could be frozen out in a sufficiently fast read-out of the annealer; in the 1D problem considered by ourselves, the domain wall behaves as a "particle in a box" whose mass is regulated by the transverse field, implying a distribution of possible domain wall positions with a peak in the middle of the chain, unlike the flat distribution expected for the ideal classical limit. Therefore, quantum fluctuations can cause quantum annealers to sample - in interesting ways - ground states unfairly [46, 47, 48, 49, 50], and such effects can sometimes be used in a beneficial way [51, 52]). However, we conclusively demonstrate that the effect observed here is classical in origin, both through numerical simulation and experiments using different runtimes. The reason that this system is dominated by classical rather than quantum effects is that the system equilibrates quickly, as has been independently observed for one dimensional chains in quantum annealers in [53].

## Theoretical Analysis

There is a vast literature on the one-dimensional Ising model dealing with issues ranging from random fields in the classical limit [37] through disordered couplers and transverse fields [41], to twisted bound-

ary conditions in the clean quantum limit (see e.g. [38]). Nonetheless, we could not locate a paper which specifically addresses the domain wall distribution for the one-dimensional Ising model with twisted boundary conditions and a longitudinal random field, and what is relevant for quantum simulators, the evolution of this distribution with a transverse field. While such domain-wall distributions can be easily obtained through numerical sampling as we describe below, we provide in this section an analytical calculation in the classical limit, followed by some remarks on what could happen during the quantum annealing process.

Let us start by considering the energy contribution from the field control errors in the case of a single domain wall on the  $n$ th coupler in the chain,  $E_n = \sum_{i=1}^N \text{sign}(n - i + 0.5) \zeta_i$ . The difference in energy between two domain-wall positions is therefore  $E_n - E_m = 2 \sum_{i=m+1}^n \zeta_i$  where  $n > m$ .

Assuming that  $\bar{\zeta}_i = 0$  and  $\bar{\zeta}_i^2 = \bar{\zeta}^2$ , we note that  $\overline{E_n - E_m} = 2 \sum_{i=m+1}^n \bar{\zeta}_i = 0$ , but

$$\begin{aligned} & \overline{(E_n - E_m)(E_n - E_k)} \\ &= 4 \bar{\zeta}^2 \min(|n - k|, |n - m|) \Theta[(n - k)(n - m)], \quad (4) \end{aligned}$$

where  $\Theta$  is a Heaviside theta. Note that this formula explicitly demonstrates that the domain wall energies are correlated, even for uncorrelated fields. Also note that for a Gaussian distribution  $\bar{\zeta}^2 = \sigma_\zeta^2$ . The probability of finding a domain wall at site  $n$  in a thermal ensemble averaged over noise is given by

$$P_n = \overline{Z^{-1} e^{-\beta E_n}} = \left[ 1 + \sum_{m \neq n} e^{-\beta (E_m - E_n)} \right]^{-1}.$$

Let us now consider a high-temperature approximation to obtain an analytical formula. By expanding this probability to second order in  $\beta = \frac{1}{k_B T}$  and applying Eq. (4) we obtain

$$P_n \approx \tilde{P} + \beta^2 \bar{\zeta}^2 \frac{2}{N^2} \left( n - \frac{N+1}{2} \right)^2 \quad (5)$$

where  $\tilde{P} = \frac{1}{N} - \frac{\beta^2}{N^3} \bar{\zeta}^2 (\frac{5}{4} N^3 + N^2 + \frac{1}{6} N + 1)$ . This demonstrates that even small field control errors create a parabolic (U-shaped) distribution of domain walls. Simple, uncorrelated errors can have a strong effect on the equilibrium behavior of a simple domain-wall system. Note that this calculation relies upon

the assumption that the system is in thermal equilibrium. We justify this assumption numerically in Sec. 2.2 of the supplemental material that accompanies this manuscript. We also demonstrate other derivations at finite and zero temperature in Sec. 2.3 and 2.4 of the supplemental material. The expansion used in Eq. (5) is only guaranteed to be valid for temperatures much higher than the maximum difference in domain-wall energies,  $\beta \zeta \sqrt{N} \ll 1$ . We therefore expect that this approximation will break down for long chains, and experimentally demonstrate this breakdown in the paper.

This phenomenon is interesting as an experimental tool, because it provides a way of directly measuring the effect of the control errors on the evolution of a non-trivial Hamiltonian (i.e. with non-zero interactions between qubits). Therefore, we expect that the control errors measured this way should give a more accurate portrayal of the errors experienced in a real computation than in single qubit methods where interactions between qubits have been set to zero.

We conclude - to motivate future research - with considerations of what might happen during genuine ( $T=0$ ) quantum annealing and quenches. Most noteworthy is that for the twisted boundary conditions represented by Eq. 1 and Eq. 2, we have a domain wall which can be thought of as a particle whose mass approaches zero and size (uncertainty in position) diverges as the quantum critical point where  $A=J$  is approached (see [36] and references therein). For a finite system, the wall is a particle in a box, which is more likely in its ground state to be found at the center of the box than at the edges. As we lower the transverse field below  $J$ , we expect the random fields to cause localization to occur as this is a one-dimensional system, i.e. in a chain of length  $L$  the domain wall should be localized as soon as its quantum mechanically defined size is smaller than  $L$ . What this means is that for a quantum annealer which is truly at zero temperature, the system can become trapped in a configuration which does not minimize energy. Furthermore, the random longitudinal fields would produce a distribution of wall positions (read out via projection of individual spins onto the  $z$  axis) broader than expected for the clean limit.

## Results

Experiments were performed on a D-Wave Processor as described in Methods (and in more detail in the supplemental material), and we describe the key findings here. Firstly consider an individual instance of the Hamiltonian shown in Fig. 1 used in a quantum annealing protocol. Fig. 2 demonstrates such an experiment, in particular annealing on the same chain run repeatedly over time with no averaging either over different definitions of 0 and 1 on the qubits (gauge averaging), or over different physical chains. As with most other experiments reported here each anneal took  $20\mu s$ . The distribution of domain walls is non-uniform, as expected for local random fields even though we have tuned the qubit controls in an effort to eliminate such random fields.

We now check whether the simple classical considerations of the previous section can account for our experimental observations. To avoid effects due to local variations in qubits and couplers, we average over different chains and gauges. Fig. 2 also shows that the deviation between runs is much larger than expected for identical samples drawn from the same distribution, which can be seen by comparing the actual spread of the points with the standard error depicted in the error bars in the lower frame. This indicates that the control error has components that are faster than the time between samples. Fast errors are more difficult to detect, as well as to remove. For more discussion on this subject, see Sec. 2.6 of the supplemental material.

The difference in domain-wall probabilities in Fig. 2 is due to a combination of control errors, of the form given in Eq. 3, and coupler control errors. However, as we described in Sec. 2.1 of the supplemental material, measuring the average domain-wall distribution removes the effect of coupler errors, allowing us to measure only the field errors.

Fig. 3 displays the results from running the QPU with the final Hamiltonian corresponding to the chain configuration shown in Fig. 1, while averaging over many embedding and gauge choices. An embedding corresponds to mapping a problem on a QPU such that every variable of the problem is represented by a subset of the qubits on the QPU. Note that

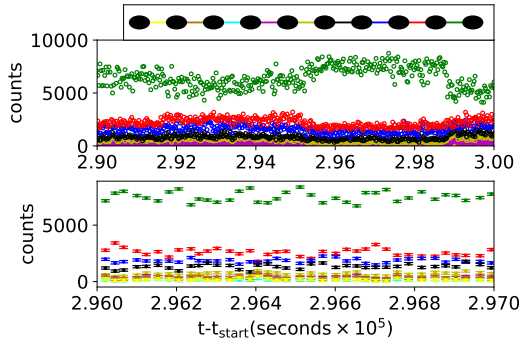


Figure 2: Experimentally observed domain-wall counts for a single embedding and gauge choice versus sample time for a 10-qubit chain (domain wall sites are color coded in cartoon). Time scales are different for top and bottom. Error bars in the bottom frame are standard error, and are suppressed in the top frame for clarity. Dashed lines in the top figure represent times when the system updates an internal self correction of biases.

chains can always be embedded in a one-to-one fashion, where every logical variable corresponds to one physical qubit; this is not true for more complicated graphs for which embedding is a more involved process [56]. Gauge choices arise due to an invariance of the target Hamiltonian under flips in the sign of a particular spin and the corresponding local field and couplings between it and other spins. This averaging is explained in the Methods section and Sec. 1.1 of the accompanying supplemental material.

The experiment now yields a U-shaped distribution, with the probability for the domain wall to be located at the very end of the chain suppressed. The suppression is predicted from well understood rf-SQUID background susceptibility effects [33], and can be removed by applying a simple linear correction; for more details see Sec. 1.2 of the supplemental material. Fig. 4 shows the behaviour of the experiments when performed on a longer chain, where the distribution deviates from parabolic due to the breakdown of the assumptions underlying Eq. (5). For longer chains it is natural to ask whether Griffiths-McCoy-Wu singularities may be playing a role in the

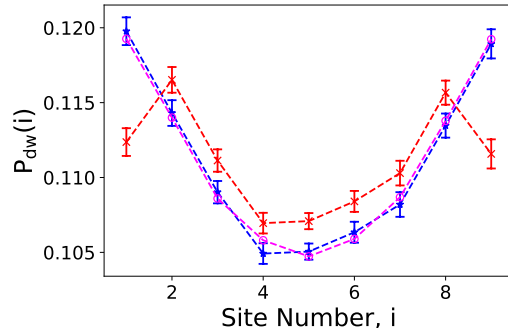


Figure 3: Domain-wall probability distributions for 10-qubit frustrated chain. Crosses are raw experimental data. Asterisks are the same with a correction applied for background susceptibility. Circles are numerically calculated data from sampling Boltzmann distributions with field noise of the form Eq. (3) with  $\frac{\sigma_z}{T} = 0.2363$ . Lines joining points are a guide to the eye.

dynamics (such effects have recently been observed in two dimensional systems using quantum annealers [54]). However, these would manifest themselves as unusual configurations such as multiple domain walls with regular spacings between them, rather than the distribution of single domain walls present in the ground state of a frustrated chain. In our experiments we predominantly observed the single-domain-wall state indicating that these effects were not playing a crucial role.

Although the theoretical predictions provide a good fit to the data, it is important to establish whether we are really justified in treating the output as a classical thermal distribution, and whether any residual quantum effects remain. It has been shown that performing quantum simulations on spin chain systems using D-Wave annealers is difficult due to the fact that a very fast quench is required to capture the dynamics. In fact simulations performed on unfrustrated spin chains in [53] suggest that a quench would need to be of order  $10^5$  times faster than currently available. As section 2.2 of the supplemental material shows, we find the same result. The simulations in [53] also suggest that the scaling of the

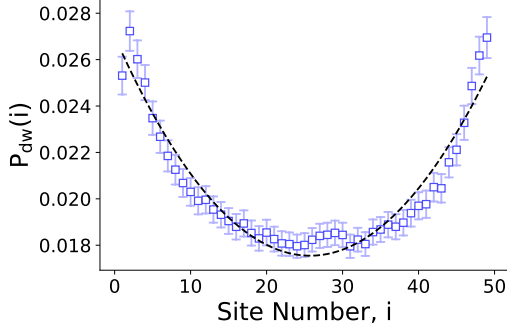


Figure 4: Domain-wall distribution for a 50-qubit chain using the same experimental setup as Fig. 3 (including background susceptibility corrections) Dashed line is a parabolic fit. Error bars are standard error.

experiments is not favourable with system size, indicating that it will actually be more difficult to observe quantum effects in longer chains than the short ones we have simulated. To further confirm that the system is very close to thermal equilibrium, we perform annealing at two very different annealing times, as depicted in Fig. 5. In this figure we see that making the run time orders of magnitude longer makes a only small difference in that the minimum of the distribution is slightly more pronounced at longer runtimes.

We next examine the effect of the weak transverse fields which are still present at the freeze time, and whether this can lead to interesting quantum effects. We assume that the freezing occurs when  $A(t) = 0.1 \text{ GHz}$ , which is reasonable based upon previous work [8], and then compare the thermal distribution with or without the transverse field present, assuming a noise of  $\frac{\sigma_\zeta}{T} = 0.24$  which can be extracted by fitting our experimental data as described later. Assuming a temperature of  $T = 15 \text{ mK} = 0.31 \text{ GHz}$ , we find the distributions in Fig. 6. The transverse field has very little effect, aside from a slight suppression of terminal site probabilities. We therefore conclude that the dominant effects observed in these experiments are indeed classical, and perform our remaining analysis from the perspective of classical thermodynamics.

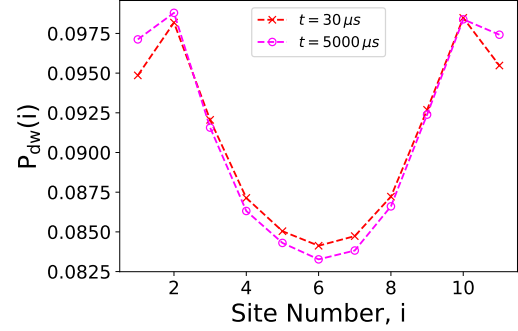


Figure 5: Domain-wall distribution for a 12 qubit chain with two different anneal times. Standard error errorbars are smaller than the depicted symbols. Background susceptibility corrections are not included.

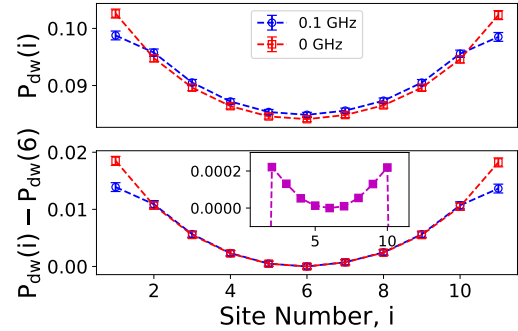


Figure 6: Top: Numerically calculated domain-wall distribution assuming thermal equilibrium in the presence or absence of a transverse field for experimentally realistic parameters. Bottom: same as top but with mid-point value subtracted to allow direct comparison, inset is difference between the two curves. Both data were taken using the same  $10^5$  random noise realizations. Error bars are standard error, and this plot uses experimentally realistic parameters  $\frac{\sigma_\zeta}{T} = 0.24$  and  $T = 15 \text{ mK} = 0.31 \text{ GHz}$ .

Returning to analysis of the 10-qubit chain, the experimental data match the numerical data obtained by Boltzmann sampling over field noise of the type in Eq. (3) with  $\frac{\sigma_\zeta}{T} = 0.24$  ( $\sigma_\zeta \approx 0.074 \text{ GHz}$ ). This fitting was performed against numerical sampling results rather than Eq. (5) to allow for higher-order corrections. Specifically, the fitting was performed by numerically sampling over disorder realizations and varying the parameter  $\frac{\sigma_\zeta}{T}$  until the least squares error with respect to the experimental distribution was minimized. By contrast, a naive estimate made by sampling uncoupled qubit polarization yields  $\frac{\sigma_\zeta}{T} = 0.13$  ( $\sigma_\zeta \approx 0.040 \text{ GHz}$ ).

The result that a naive single decoupled qubit measure of local random fields is substantially below the random fields needed to generate the non-trivial "U" distribution of domain walls for coupled qubits is a key outcome of our study. One possible explanation is that each sample is averaged over many annealing runs (each of which use the same annealing time as the domain wall experiments) and is therefore blind to any errors with a timescale less than the time to collect all the samples, which is approximately 1 second. A more sophisticated analysis based upon calculating autocorrelation via the Fourier transform (FT) of the single-qubit results yields  $\frac{\sigma_\zeta}{T} = 0.35$  ( $\sigma_\zeta \approx 0.11 \text{ GHz}$ ) (see Sec. 1.3 of the supplemental material for details) and so together with the outcome of the polarization sampling technique, brackets the result obtained from the domain wall distribution for the Ising model with interacting qubits. As with the polarization calculation, the FT experiments are performed with the coupling turned off. This method is expected to be sensitive to a wider bandwidth of errors than the naive measurement, but should still be blind to any noise faster than the Nyquist interval, which in this case is about  $178 \mu\text{s}$ . A summary of the different noise measurements can be found in table 1

Autocorrelation (FT), which has the fastest time scale, measures more error than the domain-wall technique or longer term sampling, which means that there are short-term fluctuations in uncoupled qubits which do not matter when we are dealing with the coupled qubits in the domain wall problem.

Methods based on measuring the U-shaped distri-

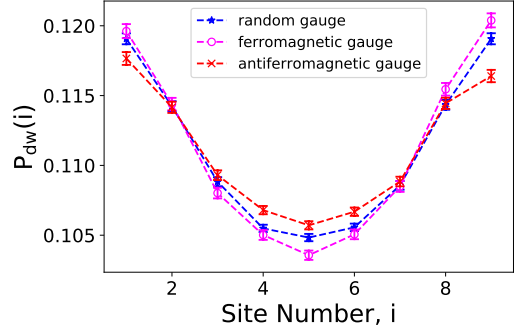


Figure 7: Domain-wall distribution with different gauge choices. X represents data taken in the gauge which all couplers are antiferromagnetic. Asterisks are averaged over random gauges. Circles are data for the gauge in which all couplers are ferromagnetic. All data in this figure have been corrected for background susceptibility.

bution can further be used to address questions about the source of the control error. For example, we can measure the coupling dependence of the field control error by fixing the gauge of the chain and averaging over only embeddings. With a fixed gauge, we must use a different embedding strategy to reduce correlations in the control errors caused by embedding to qubits in the same unit cell, see Sec. 1.1 of the supplemental material. As Fig. 7 demonstrates, the depth of the U is different depending upon the gauge, which represents strong evidence that how the couplers are set influences the local random fields. This result is consistent with measurements performed by others that indicate that ferromagnetic couplers should couple more strongly to noise [2]. Our method of measuring the coupler-dependent portion of the control error does not require operation of the control lines outside of the preprogrammed annealing schedule of the device, while the method employed by [2] does.

For the U-shaped distribution to be useful to measure field control errors requires the underlying assumption that the errors are uncorrelated. Most types of correlation between nearby qubits will be removed by the process of gauge averaging. How-



measurement technique	coupling on?	sensitive to minimum time scale	$\frac{\sigma_\zeta}{T}$	$\sigma_\zeta$ (GHz)
Domain wall	Yes	N/A	0.2363	0.074
Naive sampling	No	1 s	0.13	0.040
Fourier transform	No	178 $\mu$ s	0.35	0.11

Table 1: Summary of different noise measurement techniques and the results obtained from them.

ever, coupler-mediated errors from a shared coupler may depend on the state (ferro or anti-ferro) of the coupler [2], and therefore may contain some correlations that survive gauge averaging. We suspect that this part of the error should be relatively small because these correlations will only come from one of the 5 or 6 couplers connected to a given qubit, and only a fraction of the error from each coupler is state dependent [2].

We also have checked experimentally whether state-dependent errors have a significant effect. Fig. 8 demonstrates that the depth of the distribution does not change within statistical error when the strength of the coupling is reduced by a factor of 2. If there were a strong component of the control error which depended on the state of the couplers, we would expect a substantial difference between the depth of these two distributions. This result is consistent with the mild dependence of the outcomes on gauge choice, and reinforces the concept that dynamical effects at the longest time and smallest energy scales are responsible for the discrepancies between the effective random fields seen for interacting and non-interacting qubits.

To validate the calibration of the random fields measured via the domain wall technique relative to the single qubit methods, we use the field controls of the chip to insert Gaussian control errors with a width  $\sigma_{ext}$ . Assuming that the original control error is not affected by the additional error that we insert artificially, the two errors will be independent, and the total error will be  $\sigma_{tot} = \sqrt{\sigma_\zeta^2 + \sigma_{ext}^2}$ . The strength of the inserted control errors,  $\sigma_{ext}$  is dependent on  $t$ , in the annealing schedule specified by  $A(t)$  and  $B(t)$  and therefore the time at which the qubits become effectively ‘frozen’. It is important to note that  $\sigma_\zeta$  can also depend upon the freeze time, so dif-

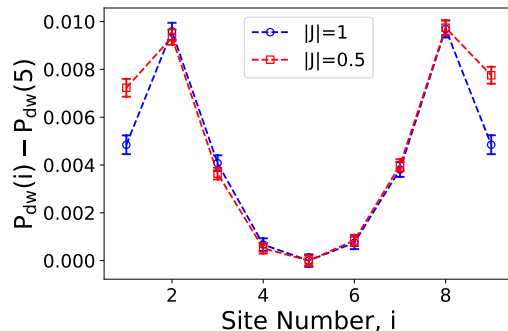


Figure 8: Difference between domain wall probability on site  $i$  from the probability that domain wall is found on site 5 for two scales of the coupling. Note that background susceptibility corrections have not been performed.

ferent freeze times with the couplings on versus off can potentially explain the deficit in the errors measured by the chain method. For our analysis we assume that the system freezes when  $A(t) = 0.1$  GHz, which is reasonable based upon previous work [8]. Fig. 9 shows the measured value of  $\sigma_{ext}$  versus the programmed value. From this figure we see that within generous errors the domain wall distributions agree with this model of the error, for which the results should appear on the diagonal indicated by the dashed blue line, while local autocorrelation measures an excess of error from the phenomenological result.

## Conclusions

We consider the performance of a real annealer for one of the simplest illustrations of magnetic frustration, namely that of a magnetic domain wall in an Ising chain constrained to have opposite spin at ei-

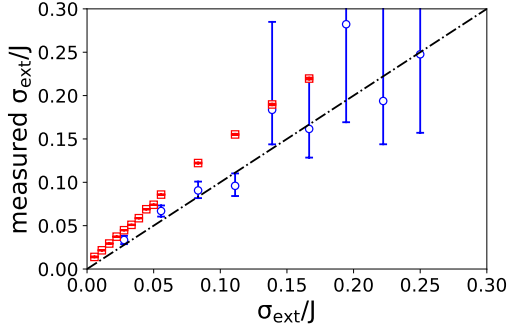


Figure 9: Plot of measured values of  $\sigma_{ext}$ , where the local random fields measured in the absence of the imposed local fields  $\sigma_{ext}$ , are subtracted according to the quadrature formula in text, versus its actual value, assuming the system freezes when  $A(t) = 0.1 GHz$ . The effective random field strength we have used is the same as before,  $\frac{\sigma_{\zeta}}{T} = 0.24$ , using at temperature of  $15 mK = 0.31 GHz$  and  $J = 1.80 GHz$ , we obtain  $\frac{\sigma_{\zeta}}{J} = 0.041$ . Blue circles are from comparing the ‘depth’ of the U with numerical sampling. Red squares are from comparing autocorrelation with the results of numerical sampling. Dot-dashed line is a guide to the eye at equal measured and applied  $\sigma_{ext}$ . For this plot we define the ‘depth’ as the ratio of the probability to find the domain wall in the middle site over the sum of all probabilities excluding terminal sites. The terminal sites are excluded to avoid having to compensate for the background susceptibility effect seen in Fig. 3.

ther end. In the absence of random fields, the wall resides on any bond with equal probability. When quantum fluctuations are present, the wall behaves as a particle in a box, which is in its ground state will have maximum probability amplitude in the middle of the chain. On the other hand, when classical random fields dominate, the distribution function for the wall becomes “U” shaped, with a minimum at the middle of the chain. We demonstrate this result with a simple analytical calculation, and then proceed to observe that it is also the generic result for the D-Wave quantum annealer. Based on the fact that we see these effects even though local random fields are zeroed with couplings between qubits tuned to zero, new random fields may be induced when the couplers are turned on to implement interacting qubit Hamiltonians. Annealers are meant to solve optimization problems, e.g. in logistics or machine learning, with many degrees of freedom. The appearance of random fields as coupling terms are turned on after zeroing local random fields acting on individual qubits can produce the usual pathologies associated with random fields in statistical physics. Most notable among these are the pinning of “domain walls” [61, 62] - corresponding to the most difficult optimization problems - will matter in systems with dimensionality higher than one. The possibility that the couplings introduce noise should not come as a surprise given that we are after all, dealing with an analog computer. It is also not unprecedented in realizations of quantum annealers: for example, local longitudinal random fields can be induced by transverse fields in magnetic systems (see [35] and references therein). We can turn a problematic but interesting effect (bug) into a benefit (feature), namely using measurements of the “U” distribution to directly measure control errors for quantum annealers.

This measure has several advantages which makes it a useful tool for understanding control errors in quantum annealing. It allows measurements to be made when couplers are active, therefore providing a more realistic estimate of the effects of control errors when solving real problems. Furthermore, the tests require no special access beyond the ability to submit problems to the device, so will be applicable for cases where users with limited access to the controls

want to characterize noise in the controls. The relative ease of performing the measurements coupled with the fact that the measurements are performed in a fundamentally different way than the standard single, decoupled qubit measurements will also make running the 1D domain wall problem a simple method for characterizing new devices. The errors detected for coupled qubits are important to characterize because it has been shown that if left unchecked, errors in the problem specification can have catastrophic effects on the result [59].

Our method runs with the standard annealing protocol, requiring no privileged access to the control lines, and measures the component of the noise which acts as control error *by construction*, with no frequency cutoff that depends on the annealing time. The second point means that the method could be used for arbitrarily long annealing times to observe deviations from the user-specified fields during the annealing process. On the other hand, should a processor be claimed to be a quantum simulator with a sufficiently rapid quench and readout, the domain wall problem will yield a distribution with a maximum rather than minimum at the centre of the chain, thus providing a qualitative test as to whether the device is classical random-field or quantum fluctuation-dominated. The cross-over between random field and quantum fluctuation-dominated regimes has been observed for model magnets [60], and we look forward to seeing a demonstration for properly programmable quantum simulators such as arrays of Josephson junctions or ion traps.

## Methods

The data in Fig. 3 were taken on the USC Information Sciences Institute Vesuvius 6 D-Wave QPU. Except where otherwise stated, these data were averaged over gauges, as well as over ways of embedding on the QPU. For more details about the embedding see Sec. 1.2 of the supplemental material. Data in Fig. 2 were taken using a QPU intermediate between the Vesuvius and Washington QPU generations made available by D-Wave Systems Inc. Unless otherwise stated all data were taken using an annealing time of

20  $\mu$ s. All individual data sets are taken with 10,000 annealing runs.

## Acknowledgments

The authors would like to thank Trevor Lanting, Murray Thom, Anatoly Smirnov, Stefan Zohren, and Jack Raymond for useful discussion. NC was supported by Lockheed Martin corporation and EPSRC fellowship EP/S00114X/1 while completing this work. TD was supported by EPSRC grant EP/K02163X/1. WV was supported by EPSRC grant EP/K004506/1. AGG was supported by EPSRC grant EP/I004831/2. The authors thank the University of Southern California for allowing access to their D-Wave 2 quantum annealer as well as D-Wave Systems Inc. for access to the intermediate-generation annealer. Collaboration with USC is supported under EPSRC grant EP/K004506/1.

## Author Contributions

NC performed the experiments. MHA and NC performed the calculations with useful assistance from AGG. MHA produced the simulations which demonstrated that the system can be treated as equilibrated. NC wrote the paper. WV performed early experiments which demonstrated the effect. PJDC and TD performed simulations which informed the early directions of the project. AGG recognized that the effect was related to order by disorder. NC and GA designed the experiment with PAW providing a particularly useful suggestion. All authors were involved in discussions of the results.

## References

- [1] Barahona, F. On the computational complexity of Ising spin glass models. *J. Phys. Math. Gen.* 15, 3241–3253 (1982).
- [2] Brooke, J., Bitko, D., Rosenbaum, T. F. & Aeppli, G. Quantum annealing of a disordered magnet. *Science* 284, 779–781 (1999).

- [3] Farhi, E. et al. A quantum adiabatic evolution algorithm applied to random instances of an NP-complete problem. *Science* 292, 472–475 (2001).
- [4] Hogg, T. Quantum search heuristics. *Phys. Rev. A* 61, 052311 (2000).
- [5] Villain, J. Bidaux, R. Carton, J. -P. Conte, R. Order as an effect of disorder *J. Phys France* 41 1263 (1980).
- [6] Boixo, S. Albash, T. Spaldalieri, F. M. Chancellor, N. Lidar, D. A. Experimental signature of programmable quantum annealing *Nature Comm.* 4, 3067 (2013).
- [7] Vinci, W. Albash, T. Mishra, A. Warburton P. A. Lidar, D. A. Distinguishing classical and quantum models for the D-Wave Device arXiv:1403.4228 (2014).
- [8] Johnson, M. W. et. al. Quantum annealing with manufactured spins. *Nature* **473**, 194-198 (12 May 2011)
- [9] Boixo, S. et. al. Quantum annealing with more than one hundred qubits. *Nature Phys.* 10, 218 (2014).
- [10] W. Vinci *et al.*, "Hearing the shape of the Ising model with a programmable superconducting-flux annealer," *Scientific Reports* 4 5703 (2014).
- [11] Harris, R. et. al. Experimental investigation of an eight-qubit unit cell in a superconducting optimization processor *Phys. Rev. B* **82**, 024511 (2010)
- [12] Santra, S. Quiroz, G. Ver Steeg, G., Lidar, D. A. MAX 2-SAT with up to 108 qubits arXiv 1307.3931 2013
- [13] Coxson, G. E. Hill, C. R. Russo J. C. Adiabatic quantum computing for finding low-peak-sidelobe codes, Presented at the 2014 IEEE High Performance Extreme Computing conference.
- [14] Choi, V. Adiabatic Quantum algorithms for the NP-Complete maximum-weight independent set, exact cover and 3SAT problems. arXiv:1004.2226 (2010)
- [15] Garnerone, S. Zanardi, P. and Lidar, D. A. Adiabatic quantum algorithm for search engine ranking. *Phys. Rev. Lett.* **108**, 230506 (2012)
- [16] Marzec, M. Portfolio optimization: applications in quantum computing, FE800 – Special Projects in Financial Engineering
- [17] Chancellor, N., Szoke, S., Vinci, W. et al. Maximum-entropy inference with a programmable annealer. *Sci Rep* 6, 22318 <https://doi.org/10.1038/srep22318> (2016).
- [18] Amin, M. H. Andriyash, E. Rolfe, J. Kulchysky, B. and Melko, R. Quantum Boltzmann machine ,arXiv:quant-ph:1601.02036 (2016).
- [19] Benedetti, M. Realpe-Gómez, J. Biswas, R. and Perdomo-Ortiz, A. Estimation of effective temperatures in quantum annealers for sampling applications: A case study with possible applications in deep learning, *Phys.Rev. A* 94, 022308 (2016).
- [20] Benedetti, M. Realpe-Gómez, J. Biswas, R. and Perdomo-Ortiz, A. Quantum-assisted learning of graphical models with arbitrary pairwise connectivity arXiv:1609.02542 (2016).
- [21] Khoshaman, A. et. al. Quantum Variational Autoencoder, *Quantum Sci. Technol.* 4 014001 (2019).
- [22] Sadeghi, H. et. al. PixelVAE++: Improved PixelVAE with Discrete Prior, arXiv:1908.09948 (2019).
- [23] Vinci W. et. al. A Path Towards Quantum Advantage in Training Deep Generative Models with Quantum Annealers, arXiv:1912.02119 (2019).
- [24] Bissell, C.C. A great disappearing act: the electronic analogue computer. In: IEEE Conference on the History of Electronics, 28-30 Jun 2004, Bletchley, UK.
- [25] Young, K.C. Blume-Kohout, R. Lidar, D. A. Adiabatic quantum optimization with the wrong Hamiltonian *Phys. Rev. A* 88, 062314 (2013).

- [26] Jordan, S. P. Farhi, E. and Shor, P. W. Error-correcting codes for adiabatic quantum computation *Phys. Rev. A* 74, 052322 (2006).
- [27] Lidar, D. A. Rezakhani, A. T. and Hamma, A. Adiabatic approximation with exponential accuracy for many-body systems and quantum computation. *J. Math. Phys* **50**, 102106 (2009)
- [28] Lidar, D. A. Towards Fault Tolerant Adiabatic Quantum Computation *Phys. Rev. Lett.* 100, 160506 (2008).
- [29] Young, K. C. Sarovar, M. and Blume-Kohut, R. Error Suppression and Error Correction in Adiabatic Quantum Computation: Techniques and Challenges *Phys. Rev. X* 3, 041013 (2013).
- [30] Quiroz, G. and Lidar, D. A. High-fidelity adiabatic quantum computation via dynamical decoupling *Phys. Rev. A* 86, 042333 (2012).
- [31] Ganti, A. Onunkwo, U. and Young, K. A family of  $[[6k, 2k, 2]]$  codes for practical, scalable adiabatic quantum computation arXiv:1309.1674 (2013).
- [32] Matsuura, S. Nishimori, H. Vinci, W. and Lidar, D. A. Nested quantum annealing correction at finite temperature: p-spin models. *Phys. Rev. A* 99, 062307 (2019).
- [33] Harris, R. et. al. *Physical Review B* 81, 134510 (2010)
- [34] Kumar, P. et. al. Origin and Reduction of  $1/f$  Magnetic Flux Noise in Superconducting Devices *Phys. Rev. Applied* 6, 041001 (2016).
- [35] Silevitch, D., Bitko, D., Brooke, J. et al. A ferromagnet in a continuously tunable random field. *Nature* 448, 567–570 (2007). <https://doi.org/10.1038/nature06050>
- [36] Brooke, J., Rosenbaum, T. and Aeppli, G. Tunable quantum tunnelling of magnetic domain walls. *Nature* 413, 610–613 (2001).
- [37] Bruinsma, R. and Aeppli, G. One-Dimensional Ising Model in a Random Field *Phys. Rev. Lett.* 50, 1494 (1983).
- [38] Campostrini, M. Pelissetto, A. and Vicar, E. Quantum transitions driven by one-bond defects in quantum Ising rings *Phys. Rev. E* 91, 042123 (2015).
- [39] Pudenz, K. L. Albash, T. and Lidar, D. A. Error corrected quantum annealing with hundreds of qubits, *Nature Comm.* 5, 3243 (2014).
- [40] Fisher D. S. Random transverse field Ising spin chains *Phys. Rev. Lett.* 69, 534 (1992).
- [41] Fisher D. S. Critical behavior of random transverse-field Ising spin chains *Phys. Rev. B* 51, 6411 (1995).
- [42] Chancellor, N. Domain wall encoding of discrete variables for quantum annealing and QAOA, *Quantum Science and Technology* 4 045004 (2019).
- [43] Abel, S. Chancellor, N. and Spannowsky, M. Quantum computing for quantum tunneling *Phys. Rev. D* 103, 016008 (2021).
- [44] Chen, J. Stollenwerk, T. Chancellor, N. Performance of Domain-Wall Encoding for Quantum Annealing. arXiv:2102.12224 (2021).
- [45] Berwald, J. Chancellor, N. Dridi, R. Understanding domain-wall encoding theoretically and experimentally. arXiv:2108.12004 (2021).
- [46] Ground-state statistics from annealing algorithms: quantum versus classical approaches. *New Journal of Physics*, 11(7):073021, (2009).
- [47] Matsuda, Y. Nishimori, H. and Katzgraber, H. G.. Quantum annealing for problems with ground-state degeneracy. *Journal of Physics: Conference Series*, 143:012003, (2009).
- [48] Mandra, S. Zhu, Z and Katzgraber, H. G. Exponentially Biased Ground-State Sampling of

- Quantum Annealing Machines with Transverse-Field Driving Hamiltonians. *Physical Review Letters*, 118(7):070502, (2017).
- [49] Könz, M. S. Mazzola, G. Ochoa, A. J. Katzgraber, H. G. and Troyer, M. Uncertain fate of fair sampling in quantum annealing. *Physical Review A*, 100(3):030303, (2019).
- [50] Kumar, V. Tomlin, C. Nehrkorn, C. O'Malley, D and Dulny J. III. Achieving fair sampling in quantum annealing, arXiv:2007.08487 (2020).
- [51] Zhang, B.H., Wagenbreth, G., Martin-Mayor, V. et al. Advantages of Unfair Quantum Ground-State Sampling. *Sci. Rep.* 7, 1044 (2017).
- [52] Chancellor, N. Fluctuation-guided search in quantum annealing. *Phys. Rev. A* 102, 062606 (2020).
- [53] Izquierdo, Z. G. Albash, T. and Hen, I. Testing a quantum annealer as a quantum thermal sampler arXiv:2003.00361 (2020).
- [54] Nishimura, K. Nishimori, H. and Katzgraber, H. G. Griffiths-McCoy singularity on the diluted Chimera graph: Monte Carlo simulations and experiments on quantum hardware *Phys. Rev. A* 102, 042403 (2020).
- [55] Childs, A. M. Farhi, E. and Preskill, J. Robustness of adiabatic quantum computation *Phys. Rev. A* 65, 012322 (2001).
- [56] Fang, Y., Warburton, P.A. Minimizing minor embedding energy: an application in quantum annealing. *Quantum Inf Process* 19, 191 (2020). <https://doi.org/10.1007/s11128-020-02681-x>
- [57] Trevor Lanting, D-Wave Systems Inc. private communication
- [58] Raymond, J. Yarkoni, S. Andriyash, E. Global warming: temperature estimation in annealers. *Frontiers in ICT* 3, 23 (2016).
- [59] Pearson, A. et al. Analog errors in quantum annealing: doom and hope. *npj Quantum Inf* 5, 107 (2019).
- [60] M. A. Schmidt, D. M. Silevitch, G. Aeppli, and T. F. Rosenbaum Using thermal boundary conditions to engineer the quantum state of a bulk magnet *PNAS* 111 (10) 3689-3694 (2014)
- [61] Bruinsma, R. and Aeppli, G. Metamagnets and frustration *Phys. Rev. B* 29, 2644 (1984)
- [62] Villain, J. Nonequilibrium "Critical" Exponents in the Random-Field Ising Model *Phys. Rev. Lett.* 52, 1543 (1984).

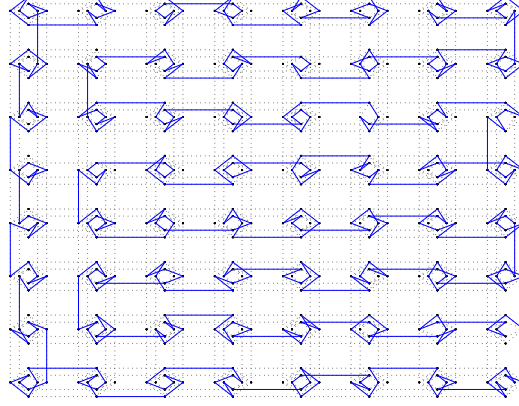


Figure 10: Periodic chain spanning the entire QPU for a single embedding. Dotted lines indicate allowed connections while solid lines show the connections that are used.

# Supplemental material

## 1 Supplemental Methods

### 1.1 Gauge and embedding averaging

#### High-Density Embedding

Eliminating of systematic biasing effects on the QPU is crucial for this kind of study. We use two techniques to counteract such effects. The first technique is to average over the local  $\mathbb{Z}_2$  gauge on each qubit. For this technique we select each qubit within a given problem instance and with a 50% probability either do nothing or flip the sign of all bonds and fields related to that qubit.

The second technique is to average over different ways of mapping the spin chain Hamiltonian to the graph of the QPU. We will refer to this mapping as an embedding. To create a random embedding, we first create a periodic chain that spans the entire QPU with randomly selected bonds as seen in Fig. 10. Starting at a random point on this chain, we then cut as many chains of the desired length as is possible. The results of this process plus gauge averaging are shown in Fig. 11.

#### Low-Density Embedding

When the data is gauge averaged, any correlation in the noise caused by physical proximity of qubits within the unit cells is removed by the random gauge. However, data that are not gauge averaged do not have this protection, and therefore should be embedded in a way that minimizes the extent to which unit cells are shared. Fig. 12 gives an example of one such embedding. Fig. 13 shows that data collected using the high-density embedding scheme (as shown in Fig. 11) but without gauge averaging do not have the U-shaped

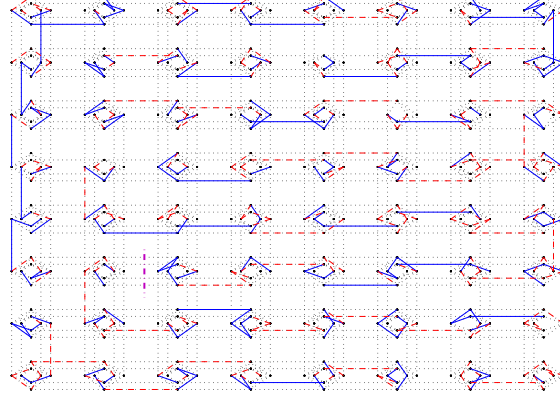


Figure 11: Final embedding produced from the periodic chain shown in Fig. 10. Solid lines are ferromagnetic bonds, dashed are antiferromagnetic. The dot-dashed line indicates the location of the initial cut.

bias found with gauge averaging.

## 1.2 Background Susceptibility Correction

We have used the model of background susceptibility used in [1] which has the form

$$J'_{ij} = \chi \sum_k J_{ik} J_{jk} \quad h'_i = \chi \sum_k J_{ik} h_k, \quad (6)$$

using the convention that  $H(t) = B(t)(-\sum_{ij} J_{ij} \sigma_i^z \sigma_j^z + \sum_i h_i \sigma_i^z) - A(t) \sum_{i=1}^N \sigma_i^x$ . This imperfection has the effect of increasing the energy of the terminal domain-wall sites by a value proportional to  $J(h - J)$ , while leaving all other site energies unchanged. To compensate for background susceptibility, we assume that the system is in a Boltzmann state at the freeze time and further approximate that the effect of the background susceptibility is linear, such that

$$P_{dw}(1) \rightarrow P_{dw}(1) \left(1 + \frac{B(t_{freeze})}{k_B T} \chi J(h - J)\right). \quad (7)$$

A similar approximation is made for  $P_{dw}(N - 1)$ .

## 1.3 Field errors

Let us first consider uncoupled qubits with no applied field. In this case, the only contribution will be from the control errors,

$$H = \zeta \sigma^z. \quad (8)$$



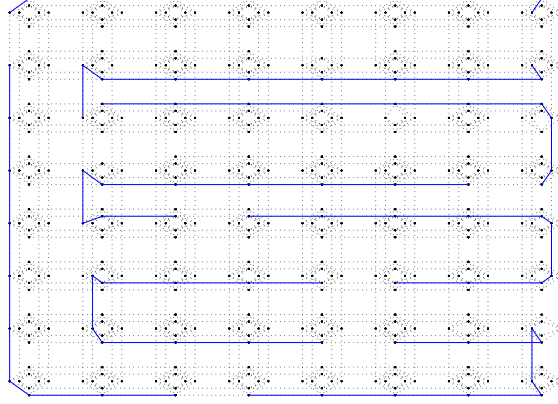


Figure 12: Embedding with a lower qubit density, which minimizes the number of qubits in the same unit cell.

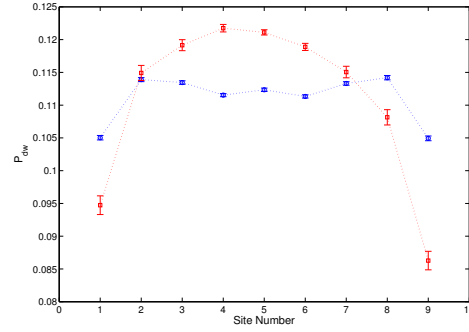


Figure 13: Domain-wall probability versus site number for high-density embeddings without gauge averaging. Circles are antiferromagnetic gauge results for dense embeddings while squares are ferromagnetic chain results using this embedding.

Single measurements of the qubit will be  $\pm 1$  and, assuming a thermal distribution, will take the form,

$$P_{\pm} = \left[1 + e^{\pm \zeta/T}\right]^{-1} = \frac{1}{2} \left[1 \mp \frac{\zeta}{T}\right] + O\left(\frac{\zeta^3}{T^3}\right). \quad (9)$$

We define the symmetrized correlation function

$$C(t) = \frac{1}{2} \langle \sigma^z(t) \sigma^z(0) + \sigma^z(0) \sigma^z(t) \rangle. \quad (10)$$

For two samples taken at different times, we therefore expect the correlation to be

$$C_{ij} = \frac{\overline{\zeta_i \zeta_j}}{T^2}. \quad (11)$$

Making use of the Fourier transform we can define the correlation spectral density for the control errors

$$S_{\zeta}(f_k) = T^2 S(f_k) = T^2 \frac{|s_k|^2}{N f_{\text{sampling}}}, \quad (12)$$

where  $f_{\text{sampling}} = 1/\delta t$  is the sampling frequency and  $N$  is the number of samples. The rms value of the noise is therefore

$$\begin{aligned} \overline{\zeta^2} &\approx \frac{1}{N} \overline{\zeta_j \zeta_{j+1}} \\ &\approx \frac{T^2}{N^3} \sum_j \sum_{k,k'} \tilde{s}_k \tilde{s}_{k'} e^{2\pi i [(j-1)(k-1) - j(k'-1)]/N} \\ &= \frac{T^2}{N^2} \sum_{k=1}^N |\tilde{s}_k|^2 e^{-2\pi i (k-1)/N}. \end{aligned}$$

## 2 Supplemental Discussion

### 2.1 Analytical and Numerical Demonstration that the Effect of Coupler Errors are Negligible

In contrast to the calculation for field errors, let us consider the effect of coupler control errors in the form  $H = \sum_i \zeta_i^{(J)} \sigma_i^z \sigma_{i+1}^z$ . In this case the energy contribution from the control errors is given by

$$E_n^{(J)} = 2 \zeta_n^{(J)}. \quad (13)$$

By inserting this energy into

$$P_n = \overline{Z^{-1} e^{-\beta E_n}} = \left[ 1 + \sum_{m \neq n} e^{-\beta (E_m - E_n)} \right]^{-1}$$

and assuming that  $\sum_{m \neq n'} e^{-2\beta(\zeta_m^{(J)} - \zeta_n^{(J)})} < 1$ , we can write

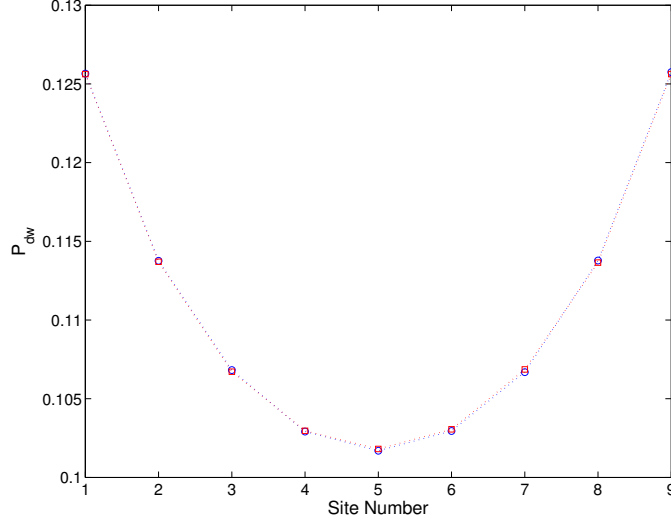


Figure 14: Plots of domain-wall distribution from numerical sampling with field errors of  $5\% J_{max}$  without coupler errors (circles), and with coupler errors of  $5\% J_{max}$  (squares).

$$\begin{aligned}
P_n &= \overline{\left[ 1 + \sum_{m' \neq n'} e^{-2\beta(\zeta_{m'}^{(J)} - \zeta_{n'}^{(J)})} \right]}^{-1} \\
&= \sum_k (-1)^k \overline{\left[ \sum_{m \neq n} e^{-2\beta(\zeta_m^{(J)} - \zeta_n^{(J)})} \right]}^k \\
&= \sum_k (-1)^k (N-1)^k = \frac{1}{N},
\end{aligned} \tag{14}$$

where we have assumed that  $\overline{\zeta_i^{(J)}} = 0$  and  $\overline{(\zeta_i^{(J)})} = \overline{(\zeta^{(J)})}$ , and therefore that  $\overline{(\zeta_m^{(J)} - \zeta_n^{(J)})^q} = 0$  for any  $q > 0$ . Unlike field-control errors, which effect the domain-wall distribution even at infinitesimal levels, coupler-control errors have no effect provided that  $\sum_{m \neq n'} e^{-2\beta(\zeta_m^{(J)} - \zeta_n^{(J)})} < 1$  and the system remains in the single domain wall sector.

As a further check that coupler errors can be neglected, we simply compare the results of numerically sampling with no coupler errors to those from sampling with coupler errors of  $5\% J_{max}$ . As Fig. 14 demonstrates, the difference between the two cases is completely negligible.

## 2.2 Justification for Treating the System as Equilibrated

Modeling an equilibrium quantum system is much less computationally expensive than simulating the full dynamics of the quantum annealing process. Given the relative simplicity and small size of the Hamiltonian

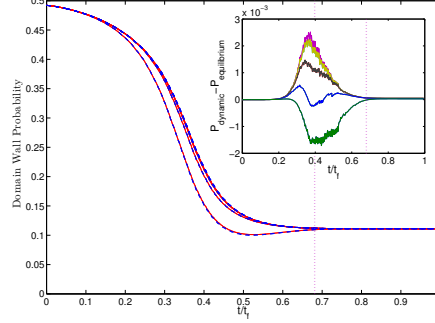


Figure 15: Comparison of open quantum system simulation of a 10 qubit chain based on the Redfield equation of annealing process (dashed) with equilibrium values at the physical temperature of the QPU (solid). Dotted line indicates freeze time. The inset shows the difference between the expected domain-wall probability in the two models. The maximum difference between these two models is of the order  $10^{-3}$ . Note that both plots contain five datasets (although there are 9 potential domain wall cites symmetry means there are only 5 unique values), but some are obscured in the main plot. Parameters for this simulation are set to match the experimental parameters in fig. 3 of the main paper.

under consideration, it is reasonable to suspect that the bath will drive the system into equilibrium relatively quickly. This assumption should be checked however. As Fig. 15 shows, Redfield-formalism open-quantum-system simulations predict that the system will in fact be very close to equilibrium at all times, including the freeze time.

### 2.3 More elaborate finite temperature calculation

Let us consider a thermal average over instances of uncorrelated random field noise. In this case, the contribution of field control errors to the energy of a domain wall between qubit  $n$  and  $n + 1$  is

$$E_n = \sum_{i=1}^n \zeta_i - \sum_{i=n}^N \zeta_i. \quad (15)$$

From this formula we observe that  $|E_i - E_j| \propto \sqrt{|i - j|}$ . Even though the fields,  $\zeta$  are not correlated, the domain-wall energies  $E$  are such that close domain walls have similar energies.

To calculate the domain-wall distribution we can take advantage of the fact that  $\langle \zeta_i \rangle = \sum_{m=1}^{N-1} P(m) \int d\vec{\zeta} P(\vec{\zeta}|m) \zeta_i = 0$ , where  $i$  indexes the fields over sites and  $m$  is the domain wall location. If the integral  $\int d\vec{\zeta} P(\vec{\zeta}|m) \zeta_i$  can be performed, we can therefore obtain a set of linear equations which, coupled with the fact that  $\sum_{m=1}^{N-1} P(m) = 1$ , can be solved for  $P(m)$ , the domain wall probability.

Let us consider what the average values of the field errors will be given that the domain wall is found on site  $m$ ,

$$\langle \zeta_n \rangle_m = \int d\vec{\zeta} P(\vec{\zeta}, m) \zeta_n = \int d\vec{\zeta} P(m|\vec{\zeta}) P(\vec{\zeta}) =$$

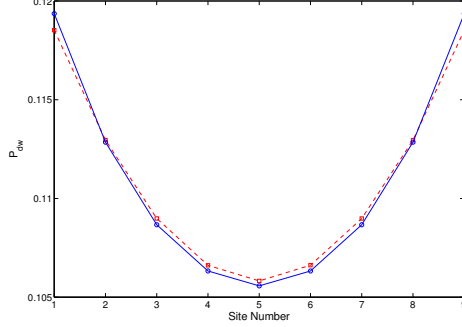


Figure 16: Calculated domain-wall distribution for 10 spin frustrated chain with a discrete distribution with  $p(\zeta) = \frac{1}{2}(\delta(\zeta - \sigma_\zeta) + \delta(\zeta + \sigma_\zeta))$  and  $\sigma_\zeta = 0.2T$ . Circles are exact results from exhaustively summing while squares are the approximate result from using Eq. 17.

$$\int d\vec{\zeta} \frac{\zeta_n \exp(-E_n(\{\vec{\zeta}\})\beta) \prod_i p(\zeta_i)}{Z(\vec{\zeta}) \mathcal{N}_m}. \quad (16)$$

In this equation  $\beta$  is the inverse temperature.  $Z(\vec{\zeta}) = \sum_{i'=1}^N \exp(-E_n(\{\vec{\zeta}\})\beta)$  and  $\mathcal{N}_m = \int d\vec{\zeta} \frac{\exp(-E_n(\{\vec{\zeta}\})\beta) \prod_i p(\zeta_i)}{Z(\vec{\zeta}) P(m)}$  is a normalization factor.  $p(\zeta)$  is the probability distribution for  $\zeta$ . Performing the multi-dimensional integral in Eq. 16 is prohibitively difficult for most choices of  $p(\zeta)$ , although it can be solved exactly in the case of  $p(\zeta) = \frac{1}{2}(\delta(\zeta - \sigma_\zeta) + \delta(\zeta + \sigma_\zeta))$ . We can however consider a simplified version of Eq. 16 by replacing the values of all but one of the fields with their mean values

$$\langle \zeta_n \rangle_m = \frac{\int d\zeta_n \frac{\zeta_n \exp(-(E_n(\{\vec{\zeta}\}))\beta) p(\zeta_m) \prod_{i \neq m} \delta(\zeta_i - \langle \zeta_i \rangle)}{\sum_{m'} \exp(-(E_n(\{\vec{\zeta}\}))\beta) p(\zeta_{m'}) \prod_{i \neq m} \delta(\zeta_i - \langle \zeta_i \rangle) \mathcal{N}_m}}. \quad (17)$$

Eq. 17 can be solved as long as we can solve  $\int d\zeta \frac{\zeta \exp(\pm \zeta \beta)}{Z(\zeta)} p(\zeta)$ . This integral is now straightforward to compute.

As a test of this method, let us consider  $p(\zeta) = \frac{1}{2}(\delta(\zeta - \sigma_\zeta) + \delta(\zeta + \sigma_\zeta))$  and compare the approximation in Eq. 17 to the exhaustive sum of exponentially many terms in Eq. 16. Fig. 16 demonstrates that this method works well in the temperature regime which the D-Wave chip operates. We also found a similar calculation technique which works well at zero temperature and can be found in Sec. 2.4.

## 2.4 Zero temperature calculation

Solving the zero-temperature case amounts to finding the probability that a given domain-wall site has the lowest energy given random field noise. We now calculate this probability by examining the probability that progressively further sites will have a greater energy than the original site (site 0 in our notation). We are

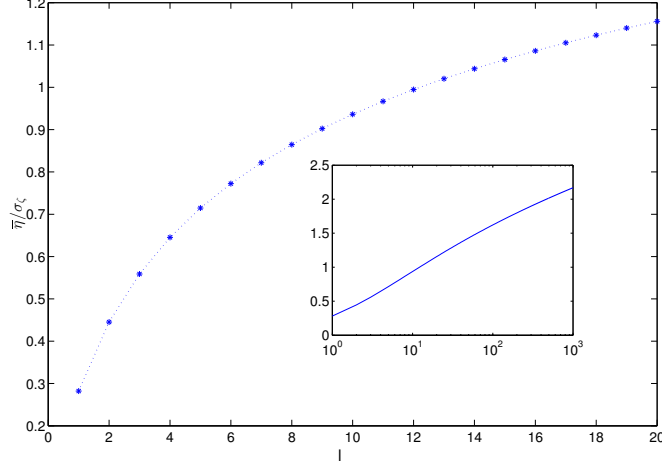


Figure 17: Mean energy of a site versus distance from original site given that no sites between them have a lower energy than the original. Inset: Lin-Log scale.

interested in the case where *no sites* have lower energy than the original. We introduce the mean energy at a site given this constraint,

$$\bar{E}_l = \int d\vec{\zeta} \epsilon E_l(\vec{\zeta}) P(\vec{\zeta} | E_0(\vec{\zeta}) < E_i(\vec{\zeta})) \forall 0 < i < l.$$

Using in a Gaussian for  $P(\vec{\zeta})$ , we now approximate the probability that a given site has a greater energy than site 0,

$$P_{>}(\bar{E}, \sigma_\zeta) \approx \int d\vec{\zeta} \Theta(E_l(\vec{\zeta}) + \bar{E}_l) P(\vec{\zeta}) = \frac{1}{\sqrt{\pi}\sigma_\zeta} \int_0^\infty d\epsilon \exp\left(-\frac{(\epsilon - \bar{E})^2}{\sigma_\zeta^2}\right) = \frac{1}{2} \left(1 + \operatorname{erf}\left(\frac{\bar{E}}{\sigma_\zeta}\right)\right), \quad (18)$$

where  $\Theta$  is the Heaviside theta.

We define  $\bar{E}$  recursively in the following way:

$$\bar{E}_l = \frac{1}{\sqrt{\pi}\sigma_\zeta} \int_0^\infty d\epsilon \epsilon \exp\left(-\frac{(\epsilon - \bar{E}_{l-1})^2}{\sigma_\zeta^2}\right) = \frac{1}{2} (\bar{E}_{l-1} (1 + \operatorname{erf}(\frac{\bar{E}_{l-1}}{\sigma_\zeta})) + \frac{\sigma_\zeta}{\sqrt{\pi}} \exp(-\frac{\bar{E}_{l-1}^2}{\sigma_\zeta^2})). \quad (19)$$

This recursive calculation can readily be performed by a computer algebra system yielding the results shown in Fig. 17.

Once the mean site energies are known, we can use Eq. 18 to calculate the relative probabilities that a given site will have the lowest energy by realizing that

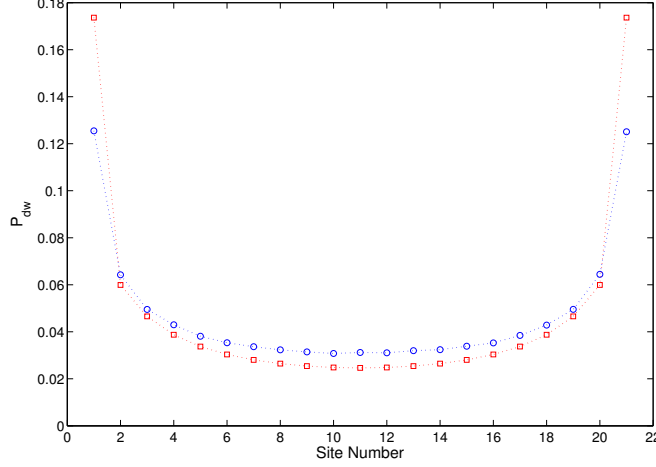


Figure 18: Domain-wall probability versus site number. Circles are the results from numeric sampling at  $\sigma_\zeta = 0.01 T$ , while squares are the zero temperature recursive solution.

$$P_{min}(n) \propto \prod_{m \neq n}^{N-1} P_{>}(\bar{E}_{|n-m|-1}, \sigma_\zeta). \quad (20)$$

As Fig. 18 shows, this approximation gives a result which is quite close to the one we obtain by numerical sampling, indicating that it captures most of the important underlying physics.

## 2.5 More on error timescales and effectiveness of shims

It is natural to ask whether the relevant field control errors occur with a short or long timescale. Long timescale errors can be removed relatively easily because they need to be measured and corrected relatively less frequently. There is in fact already an effort to correct for these implemented on the QPU. Each hour the software computes the solution to a problem with all fields and couplers turned off, from this the software estimates and compensates for the fields. This process is called a shim.

An interesting quantity to examine related to the effectiveness of the shims is the mean polarization taken between two shims;  $\langle \sigma_i^z \rangle_{shim} = \frac{1}{n_{run}} \sum_{run \in shim} \langle \sigma_i^z \rangle_{run}$ . Because it is averaged over the short timescale control errors, this quantity tells us about how effective a shim was at removing errors that are on a timescale of one hour or longer. However, we can probe at least part of the short timescale control errors by taking the average magnitude of deviations from this value,

$$\langle |\langle \sigma_i^z \rangle_{run} - \langle \sigma_i^z \rangle_{shim}| \rangle_{shim} = \frac{1}{n_{run}} \sum_{run \in shim} |\langle \sigma_i^z \rangle_{run} - \langle \sigma_i^z \rangle_{shim}|,$$

This quantity does not capture control errors that occur on timescales faster than the time it takes for the system to collect the samples, in this case roughly 1 second.

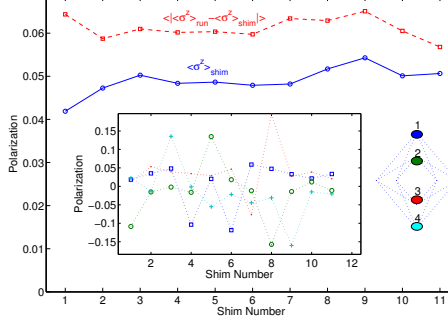


Figure 19: Experimental data for uncoupled qubits with no fields. Circles: mean of average magnitude of polarization for each shim  $|\langle \sigma_i^z \rangle_{shim}|$ . Squares: mean magnitude of difference from mean polarization within each shim (Eq. 21). Inset: mean polarization averaged over shims, shown with qubits and couplers (inactive).

A first check is whether the shims actually change the polarization direction of uncoupled qubits, as Fig. 19 (inset) demonstrates this is the case. An immediate consequence of this is that the behavior in Fig. 20, where the domain-wall probabilities on some sites are consistently higher over many shims, must not be from field control errors. Rather this is probably due to long timescale control errors in the couplers. By comparing the two lines in Fig. 19, we can see that field control errors with the time scale between 1 second and 1 hour are stronger than errors due to imperfect shims, but both are similar in magnitude.

## 2.6 More discussion of chain without averaging

Fig. 2 of the main text demonstrates that the domain-wall distribution on a single chain persists for hours. A natural next step is to examine an even longer interval and see if the behavior still persists. As Fig. 20 demonstrates, the distribution persists for days at least. A skeptical reader may ask if this behavior is typical or an anomaly. We demonstrate in Fig. 21 that such persistent distributions are typical.

As Fig. 21 shows, the mean polarization typically differs significantly from the expected value of zero. This behavior indicates that the domain walls are more probable in particular areas of the chain over the timescale of the sampling; which in this case is days. Based upon these data, we can conclude that there is a strong contribution from errors with a typical timescale that is at least days. We can also see from this figure that the majority of the variance in the domain-wall position is not from fluctuations due to the shims. Furthermore the standard deviation is much larger than that predicted due to finite sample effects. These fluctuations would be smaller than the symbol size.

## References

- [1] W. Vinci *et al.*, Hearing the shape of the Ising model with a programmable superconducting-flux annealer, *Scientific Reports* 4 5703 (2014).
- [2] T. Lanting, private communication



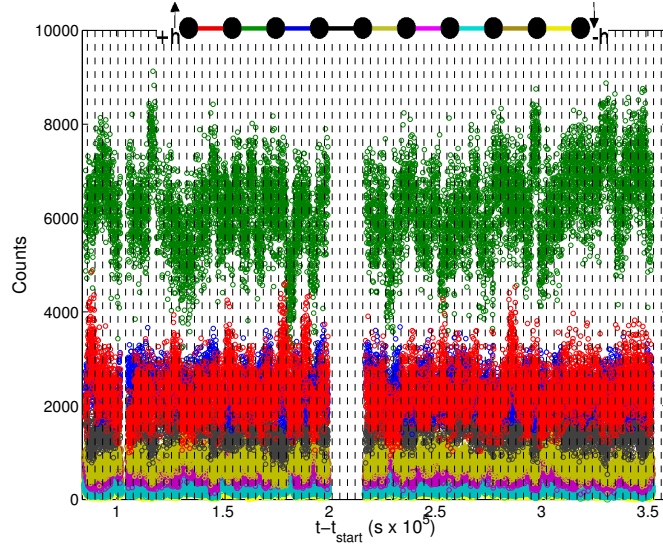


Figure 20: Same plot as Fig. 2 of the main text but plotted on a much longer timescale.

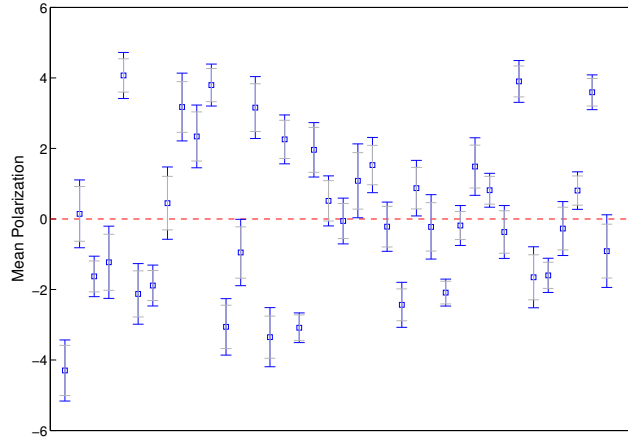


Figure 21: Mean chain polarization of whole chain where dark error bars are standard deviation for 38 different chains embedded on the same problem Hamiltonian as was used in Fig. 2 of the main paper and run for days. Given that each run consists of 10,000 samples, the expectation for randomly distributed domain walls would be to have a mean of zero and a standard deviation of 0.02. Light color error bars are the mean standard deviation from within shims. NB: error bars are standard deviation, not standard deviation of the mean. Given that the number of runs in this case was 8820, the standard deviation of the mean is smaller than the symbols.